Available online at www.sciencedirect.com

ScienceDirect

Underground Space 13 (2023) 166–182

www.keaipublishing.com/undsp

Optimization of pipe circuits in energy tunnels

Jie He [a,b], Mei Yin [c,*], Xiangyang Wei [a,b], Zhenhuang Wu [a,b]

[a] College of Civil Engineering, Tongji University, Shanghai 200092, China
[b] Key Laboratory of Geotechnical and Underground Engineering of Ministry of Education, Tongji University, Shanghai 200092, China
[c] Department of Civil and Environmental Engineering, Brunel University, Uxbridge, London UB8 3PH, UK

Received 9 January 2023; received in revised form 10 April 2023; accepted 13 April 2023
Available online 20 June 2023

Abstract

Geothermal energy is a kind of green and renewable energy. Conventionally, ground source heat pumps can be used to harvest geothermal energy from the subsurface. To reduce the initial investment, a good solution is to use tunnel linings as heat exchangers to extract/dump heat. This special infrastructure is called an energy tunnel. In addition to the thermal performance, the impact of pipe network configuration on thermal efficiency is still challenging in the design of energy tunnels. To solve this problem, this study makes the first attempt to carry out research on the optimization of pipe circuits in energy tunnels by a series of numerical analyses. A fully coupled thermo-hydraulic 3D finite element model is established to investigate the response of tunnel-soil interaction under cyclical thermal loading (initial soil temperature varies from 8 °C to 18 °C), as well as the thermal transient interactions among air, absorber pipe, tunnel linings and ground, to quantify the amount of useful heat that can be extracted from the tunnel and the ground. On the other hand, the influence of 3 various heat-carrying pipes layout is also investigated. It is found that higher heat transfer efficiency can be obtained when the entrance and exit of pipelines are located below the tunnel in the study. The spatial location of pipelines will also affect the exchanged heat output.

Keywords: Energy tunnel; Thermal efficiency; Finite element model; Heat transfer

1 Introduction

At present, energy consumption in the world is still dominated by three non-renewable fossil fuels, namely oil, coal and natural gas. Geothermal energy is a kind of green, renewable and clean energy with the characteristics of large reserves, wide distribution and good stability. Geothermal resources can be mainly divided into three types: shallow geothermal energy, hydrothermal geothermal energy and dry hot rock, according to the different modes of heat flow transmission, temperature range and exploitation. In recent decades, one of the ways to provide renewable energy for building heating and cooling is the use of ground source heat pumps (GSHPs), which take shallow surface heat as a heat source and input a small amount of energy to achieve high energy demand. When the primary heat-carrying pipes of GSHPs are installed in the tunnel linings, these elements are called energy tunnels. Since the 1980s, energy piles and walls have been gradually accepted by industry (Brandl, 2006; Amis et al., 2010; Agrawal et al., 2018; Tsagarakis et al., 2020; Zannin et al. 2021; Li et al. 2022; Song et al. 2023), but the energy tunnel is a new type of energy geo-structure. It combines the heat exchanger system with the tunnel linings and uses the heat-carrying fluid to exchange heat with the surrounding environment (soil layer, tunnel, etc.), as shown in Fig. 1. Energy tunnel heat exchangers can be arranged between primary and secondary liners (Zhang et al., 2021), or installed on the tunnel surface in combination with geotextiles (Lee et al., 2012; Tinti et al., 2017). In addition, a capillary network with a smaller diameter was used as a heat exchanger to acquire more heat power (Zhang et al., 2021). Recently, it's the tunnel lining segment

* Corresponding author.
E-mail address: mei.yin@brunel.ac.uk (M. Yin).

https://doi.org/10.1016/j.undsp.2023.04.003

Nomenclature

A	Cross-section area of pipe, m^2
A_1	Tunnel surface area, m^2
C_p	Pressure heat capacity, J/(kg·K)
c_s	Solid heat capacity, J/(kg·K)
c_w	Water heat capacity, J/(kg·K)
d_{ext}	Pipe external diameter, mm
d_h	Thermal influence radius of pipe, m
$d_{inn,surf}$	Distance from the pipeline to the inner surface of the tunnel lining, m
d_{lines}	Distance between adjacent pipelines, m
f_D	Inner wall roughness of pipe
$\boldsymbol{g}$	Acceleration of gravity, m/s^2
h_w	Groundwater table, m
h	Heat transfer coefficient, W/(m·K)
k	Thermal conductivity of heat carrier fluid, W/(m·K)
k_f	Fluid-phase thermal conductivity, W/(m·K)
k_{wall}	Pipe wall thermal conductivity, W/(m·K)
$\boldsymbol{m}$	Outer normal direction vector of boundary
n	Porosity of soil
Q	Exchanged heat power, W
$\boldsymbol{q}$	Heat flux, W/m^2
q_0	Heat flux across boundaries, W/m^2
q_f	Heat flux of fluid phase, W/m^2
q_s	Heat flux of solid phase, W/m^2
Q_A	Exchanged heat power per square, W/m^2
Q_f	Fluid exchanged heat power, W/m^3
Q_L	Exchanged heat power per length, W/m
Q_m	Magnitude of flow volume, kg/s
Q_s	Solid exchanged heat power, W/m^3
Q_{wall}	External heat exchange through pipe wall, W/m
T	Temperature of heat-carrying fluid, °C
T_{ext}	Temperature outside pipe wall, °C
T_f	Liquid-phase temperature, °C
T_{in}	Inlet liquid-phase temperature, °C
T_{out}	Outlet liquid-phase temperature, °C
T_s	Solid-phase temperature, °C
t_{pipe}	Pipe thickness, mm
$\boldsymbol{u}$	Velocity of heat carrier fluid, m/s
$_d$	Darcy's velocity, m/s
u_f	Darcy velocity of the liquid phase, m/s
z	Wall perimeter of pipe, m
α_L	Longitudinal thermal dispersivity, m
α_T	Transverse thermal dispersivity, m
κ_x	Hydraulic conductivity along x, m/s
κ_y	Hydraulic conductivity along y, m/s
κ_z	Hydraulic conductivity along z, m/s
λ_s	Solid thermal conductivity, W/(m·K)
λ_w	Fluid thermal conductivity, W/(m·K)
ρ_f	Fluid mass density, kg/m^3
ρ_w	Solid mass density, kg/m^3
μ	Dynamic viscosity of groundwater

equipped with GSHPs that is widely followed and investigated. Some successful examples of energy tunnels include Sydney Urban Tunnel (Australia) (Makasis & Narsilio, 2021), Geothermal System at Stuttgart Metro Station (Germany) (Buhmann et al., 2016), Jenbach Tunnel (Austria) (Franzius & Pralle, 2011), Turin Metro Tunnel in Italy (Barla et al., 2016, 2021), Poland Warsaw Metro Tunnel (Baralis et al., 2018), Beijing–Zhangjiakou Railway Tsinghua Park Section Tunnel (Zhu & Guo, 2019), etc.

In the case of energy tunnel, temperature changes at the inlet and outlet of heat exchangers are often used to measure the thermal efficiency of a project, the heat Q extracted or injected can be computed using the following equation:

$$Q = Q_m \cdot C_p(T_{out} - T_{in}), \quad (1)$$

where T_{in} represents the inlet temperature; T_{out} means the outlet temperature from the numerical simulation result of the pipe circuit; C_p represents pressure heat capacity and Q_m represents the magnitude of the flow volume. One-dimensional discrete feature elements were adopted to simulate the absorber pipes installed in the tunnel lining, which greatly helps with calculations. A 3D tunnel and ground model through finite element model software, such as FLAC3D (Ma et al., 2021a) and finite element subsurface FLOW system (FEFLOW) (Barla et al., 2016), is indispensable in energy tunnel research.

In winter, the heat exchange is primarily done with the tunnel environment, while most of the heat is injected into the ground in summer. It's necessary to clarify the role played in the heat transfer process of energy tunnels. Shafagh et al. (2020) developed an analytical model to investigate the thermal resistance of tunnel lining heat exchangers. Ogunleye et al. (2021) and Liu et al. (2021) assessed the thermal efficiency of energy tunnels using numerical methods. It is shown that the heat absorber pipes arranged along the axis direction of the tunnel have a higher thermal efficiency than those arranged along the circumferential direction of the tunnel. Di Donna and Barla (2016) studied the effects of ground properties (hydraulic and thermal conductivity) and ground conditions (groundwater temperature and flow velocity) on the thermal efficiency of the energy tunnel. Zhang et al. (2016) investigated the relationship between the groundwater flow rate and heat transfer performance of the energy tunnel, and found that the groundwater flow velocity has a significant effect on the subsurface temperature distribution, the air temperature variation in the tunnel and the average fluid temperature in the absorber pipes. The effect of groundwater changes the temperature field around the tunnel, which is not balanced with the formation temperature under the condition of continuous injection of heat source, but the influence scope of groundwater has not been studied.

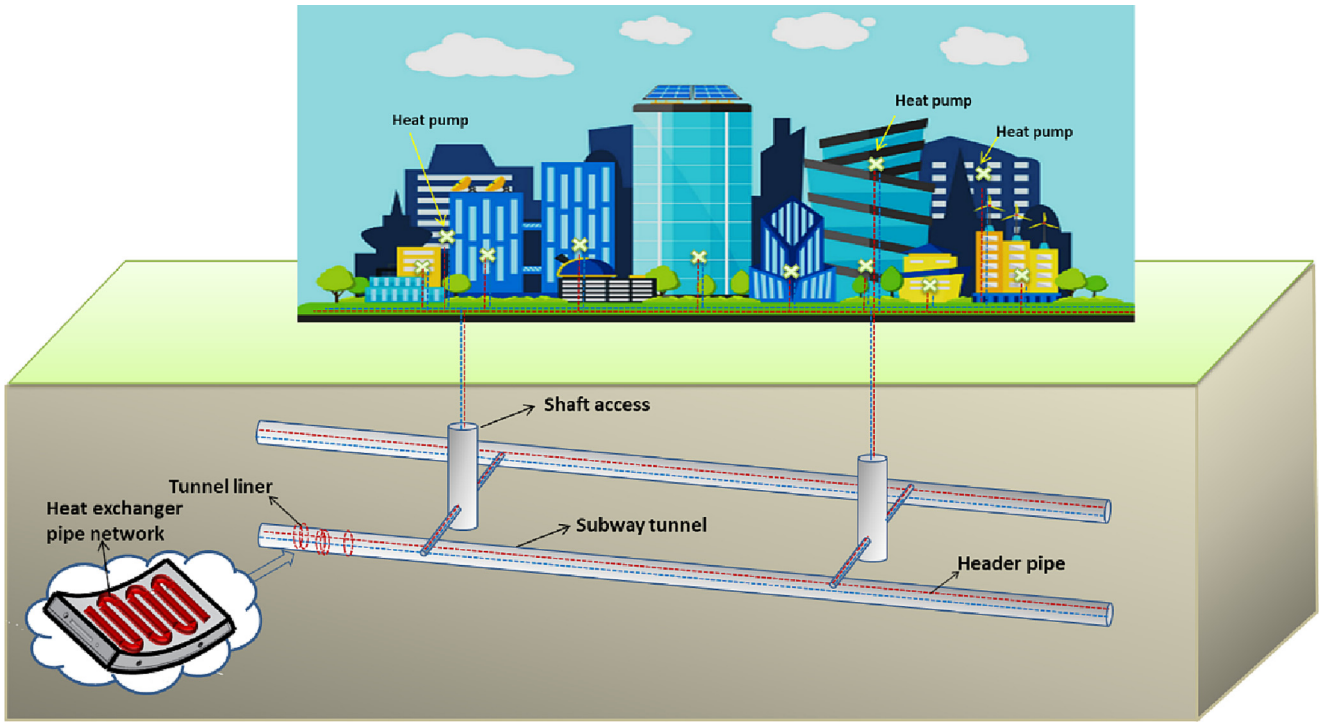

Fig. 1. Energy tunnels.

Baralis et al. (2018) performed coupled thermo-hydraulic analyses to investigate the influence of geological conditions on the efficiency of energy tunnels. Barla et al. (2019) and Insana and Barla (2020) assessed the energy performance of the energy tunnel lining by experimental and numerical studies and put forward a new concept of energy segment based on the real-scale energy tunnel tests. On the other hand, it is shown that the excessive heat generated by fast-moving trains or vehicles leads to an increase in the internal air temperature, which can be extracted by the absorber pipes of energy tunnels (Nicholson et al., 2014; Barla & Di Donna, 2018; Rowland, 2019). Although some studies have been performed on the thermal response of energy tunnels, there is no clear conclusion on how to arrange pipelines to achieve better efficiency, and the location of pipe circuits in energy tunnels as an important role in the thermal efficiency of the whole geothermal system has not been revealed. Hence, the specific research objectives of this paper are as follows: (1) a fully coupled thermo-hydraulic finite element model was established to simulate the thermal response of the energy tunnel under cyclic thermal loading; (2) the effects of groundwater flow and airflow in the tunnel on the thermal efficiency were investigated; (3) a derivative-free optimization algorithm Bobyqa was implemented to obtain the highest thermal efficiency, based on the parametric study of the route and layout of the heat absorber pipes.

2 Methodology

A fully coupled thermo-hydraulic finite element model of the energy tunnel is established in this study, which considers the heat transfer in pipes, air flow in the tunnel and groundwater flow in the soil. This model is used to simulate the long-term performance of the energy tunnel installed in the Turin Metro Line, Italy.

2.1 Mathematical formulation

(1) Mass conservation and Darcy's law

The mass conservation equation and Darcy's law can be used to describe the water flow in saturated soil. Darcy's equations describe the flow process of groundwater under the gravity and pressure gradient. The equations are as follows:

$$\frac{\partial}{\partial t}(n\rho) + \nabla \cdot (\rho \boldsymbol{u}_{\mathrm{d}}) = Q_{\mathrm{m}}, \tag{2}$$

$$\boldsymbol{u}_{\mathrm{d}} = -\frac{\kappa}{\mu}(\nabla p + \rho \boldsymbol{g}), \tag{3}$$

where ρ is the density of the groundwater; n is the porosity of the soil; $\boldsymbol{u}_{\mathrm{d}}$ is Darcy's velocity; κ is the fracture permeability, and the hydraulic conductivity model is adopted; μ is the dynamic viscosity of groundwater; $\boldsymbol{g}$ is the acceleration of gravity; and ∇p represents the tangential gradient of the water pressure.

(2) Heat transfer in pipe circuits

The heat transfer in pipe circuits involves the heat convection that occurs with the fluid flow in the pipe circuits and the heat conduction among the wall layer of the pipe circuits, the tunnel lining and the surrounding environment. The heat transfer between the heat-carrying fluid

and the environment can be expressed by the following equation:

$$\rho A C_p \frac{\partial T}{\partial t} + \rho A C_p \boldsymbol{u} \cdot \nabla T = \nabla \cdot (Ak \nabla T) + f_D \frac{\rho A}{2 d_h} |\boldsymbol{u}|^3 + Q + Q_{wall}, \quad (4)$$

$$Q_{wall} = (hz)_{eff}(T_{ext} - T), \quad (5)$$

where A is the cross-section area of the pipe; k is the thermal conductivity of the pipe heat carrier fluid; $\boldsymbol{u}$ is the velocity of the pipe heat carrier fluid; f_D is the inner wall roughness of the pipe; d_h is the thermal influence radius of the pipe; Q_{wall} means the exchanged heat through the pipe wall; $(hz)_{eff}$ is an effective value of the heat transfer coefficient (h times the wall perimeter z of the pipe). T_{ext} is the temperature outside the pipe wall; and T is the temperature of the heat-carrying fluid in the pipe circuits.

(3) Heat transfer in porous media

There are two forms of heat transfer in porous media, i.e., local thermal equilibrium and local non-thermal equilibrium. It can be understood literally that the simulation is carried out according to whether the direct temperature of each medium in the porous media system is in equilibrium ($T_f = T_s$ or $T_f \neq T_s$). The equations are as follows:

$$\rho_s C_{p,s} \frac{\partial T_s}{\partial t} + \nabla \cdot q_s = Q_s, \quad (6)$$

$$\rho_f C_{p,f} \frac{\partial T_f}{\partial t} + \rho_f C_p u_f \cdot \nabla T_f + \nabla \cdot q_f = Q_f, \quad (7)$$

where T_s is the temperature of the solid phase of the porous medium; T_f is the temperature of the liquid phase; ρ_s (ρ_f), q_s (q_f) and Q_s (Q_f) are the density, heat flux and exchanged heat power of the solid phase (liquid phase), respectively; u_f is Darcy's velocity of the liquid phase in the porous medium, which can be used for coupling calculation with Darcy's velocity field.

(4) Heat transfer model

The energy tunnel is shallowly buried in the soil layer, so the heat transfer through the thermal radiation is extremely low. The heat transfer of the energy tunnel consists of the thermal conduction between the tunnel and the ground, which could be subdivided into 4 parts: the stratum, the lining, the heat exchange pipe and the air. This is aimed to study the heat transfer between the solids, the heat convection in the fluid and the conjugate heat transfer relationship between the solids and the fluid.

Take the heat transfer model of the heat exchange pipe as an example, the heat transfer process is that the external heat transfers through the pipe wall into the pipe, and then exchanges heat with the hot fluid, as shown in Fig. 2(a). The effective heat transfer coefficient between the inner wall of the pipe and the pipe can be obtained through experimental tests. The empirical formula method is also recommended.

There are three states of solid, liquid and gas in the soil layer, which is a porous medium. Since the stratum is constant (without considering the special groundwater like hot springs), the assumption of local heat balance is adopted. Combined with the characteristics of soil, the tortuous path in the porous media will lead to heat dispersion, which can be calculated in the power-law average method, through random geometric distribution model shown in Fig. 2(b), results of which may be close to the true value.

2.2 Finite element model

The energy tunnel studied is based on the Turin Metro Line in Italy (Barla et al., 2016). The tunnel lining consists of precast concrete rings. Both the inlet and outlet heat-carrying pipes are located in the segments of the tunnel. The developed finite element model, using the finite difference software Comsol Multiphysics 5.6, mainly includes a tunnel segment with a diameter of 6.8 m and a simplified rectangular section as the stratum for analysis. As the front view of the 3D model is represented in Fig. 3(a), the model is 77.8 m high, 120 m large, and 1.4 m deep, but the center of the tunnel is 16.6 m below the ground surface. The thickness of the tunnel segment is 300 mm, and the ring's length is 1.4 m. The interior of the tunnel is assumed to be filled with air and combined with the ventilation facilities, and the airflow direction is parallel to the tunnel axis direction. Besides, there is groundwater flow perpendicular to the tunnel axis. The difference of groundwater level between the two ends of the stratum is 0.5 m, and the groundwater level is 12 m below the surface. The hydraulic and thermal parameters as well as geometrical characteristics can be found in Tables 1–3.

2.3 Initial and boundary conditions

According to the ground investigation of Italy Turin (Barla et al., 2016), the initial temperature is tested to be around 14 °C, and the groundwater levels on the left and right sides are 12.5 and 12 m below the surface, respectively. Thus, the variation of the water table and the conditions of groundwater flow in this area can be reproduced using the Darcy seepage model as shown in Fig. 4. Therefore, the groundwater flow in the horizontal direction (X) is approximately 1.5 m/d ($u_{f,x} = \kappa_x \cdot \nabla h \approx 1.5$ m/d).

Although the formation temperature is constant within a certain depth range, its initial temperature is still a function of depth. When the soil layer is closer to the surface, there will be more opportunities for heat exchange with the outside world. Therefore, the boundary conditions are set as follows. The other boundaries are set as constant temperature open boundaries, and the upstream temperature is related to the initial temperature of the ground. Regarding the upper boundary of the soil strata, it is

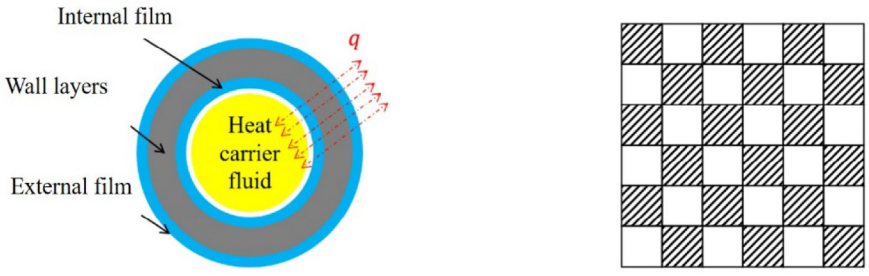

(a) (b)

Fig. 2. Heat transfer model. (a) Pipeline, and (b) ground.

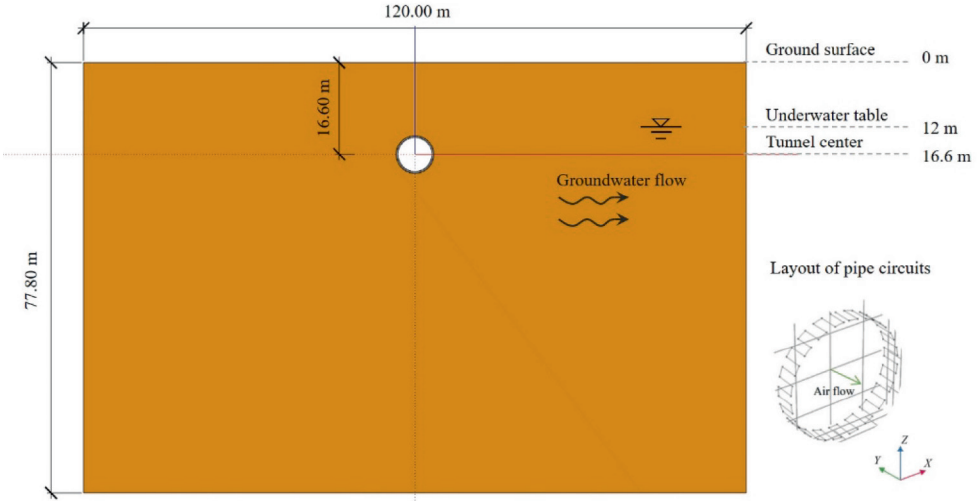

(a)

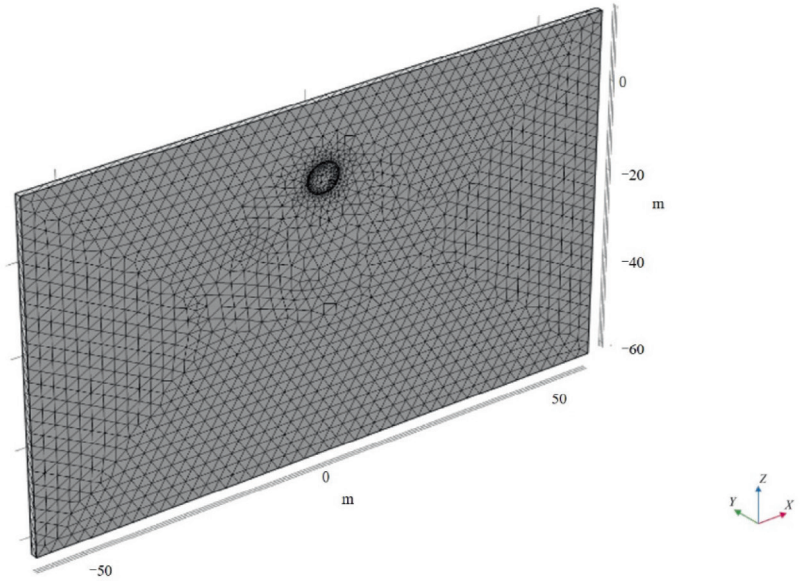

(b)

Fig. 3. Finite element model. (a) Overview of 3D model and (b) overview of mesh.

Table 1
Material property parameters used in the numerical simulation.

Material	Parameters	Symbol	Unit	Value
Ground	Porosity	n	1	0.25
	Density	ρ_s	kg/m^3	2202.60
	Thermal conductivity of the solid	λ_s	W/(m·K)	2.80
	Thermal conductivity of the fluid	λ_w	W/(m·K)	0.65
	Heat capacity of the solid	$\rho_s c_s$	MJ/(m^3·K)	2.00
	Heat capacity of the fluid	$\rho_w c_w$	MJ/(m^3·K)	4.20
Tunnel segment	Thermal conductivity of the solid	λ_s	W/(m·K)	2.30
	Heat capacity	$\rho_s c_s$	MJ/(m^3·K)	2.19
	Density	ρ_s	kg/m^3	2300.00
Pipe circuit	External diameter	d_{ext}	m	24.00
	Pipe wall thickness	t_{pipe}	mm	2.00
	Heat carrier fluid velocity	v	m/s	0.40
	Fluid-phase thermal conductivity	k_f	W/(m·K)	0.58
	Pipe wall thermal conductivity	k_{wall}	W/(m·K)	0.38
	Volumetric heat capacity	$\rho_w c_w$	MJ/(m^3·K)	4.20

Table 2
Hydraulic parameters used in the numerical simulation.

Parameters	Symbol	Unit	Value
Horizontal hydraulic conductivity	$\kappa_x = \kappa_z$	m/s	4.15×10^{-3}
Vertical hydraulic conductivity	κ_y	m/s	2.075×10^{-4}
Groundwater table	h_w	m	12

Table 3
Geometrical and technical characteristics for the numerical model.

Ground	Value	Unit	Tunnel segment	Value	Unit
Large	120.00	m	Diameter	6.80	m
High	77.80	m	Segment thickness	300.00	mm
Deep	1.40	m	Ring length	1.40	m
The groundwater level below the surface	12.00	m	Buried depth	16.60	m

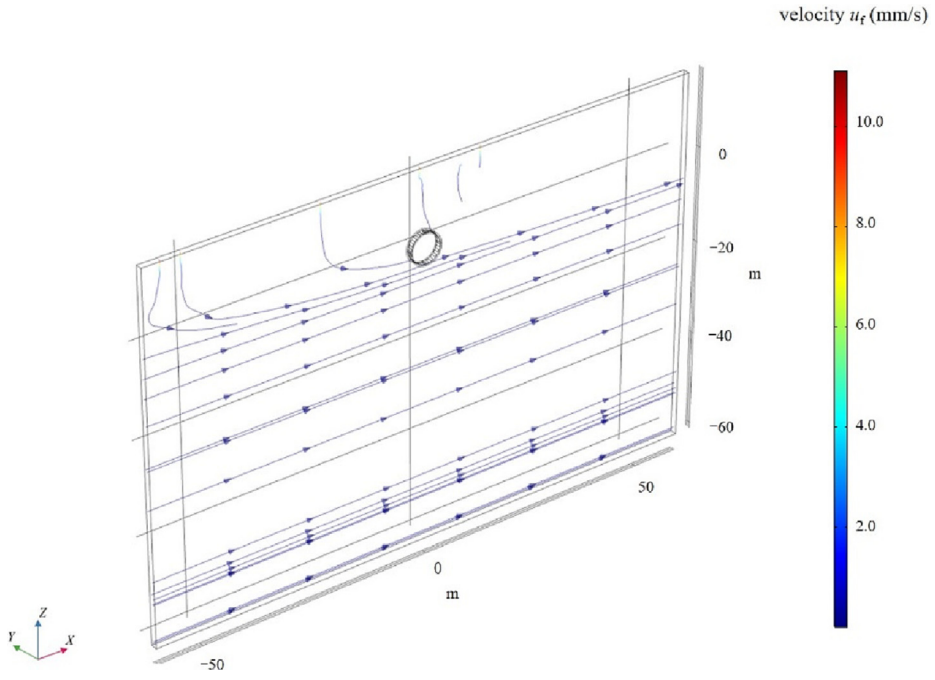

Fig. 4. Diagram of Darcy's law flow field.

assumed to be in contact with the surface atmosphere, which is consistent with the characteristics that the temperature of the stratum increases with the depth. Therefore, the upper boundary of the finite element model is set as the boundary condition of convective heat flux. The equation is as follows:

$$-m \cdot q = q_0, \tag{8}$$

where $\boldsymbol{m}$ is the outer normal direction vector of the boundary; q_0 is heat flux across the boundary.

At the same time, to consider the impact of air inside the tunnel, the ambient data of Turin from the ASHRAE standard is adopted in Fig. 5 (ASHRAE is short for American Society of Heating, Refrigerating and Air-Conditioning Engineers). It is assumed that the air inside the tunnel flows freely and exchanges with the air in the external atmospheric environment. The air velocity inside the tunnel is set to be 0.1 m/s, and the direction is parallel to the tunnel axis, as shown in Fig. 3(a). Barla et al. (2016) uses h_{eff} (the equivalent thermal resistance) to calculate the conjugate heat transfer of air, while it's calculated with the air velocity. The air velocity of 0.1 m/s is the closest to the numerical simulation results. At the same air velocity (0.1 m/s), the deviation from the heating mode is about 3%, while that from cooling mode is less than 0.1%.

The initial value of the air temperature inside the tunnel is set to be 17 °C in winter and 30 °C in summer. The simulation of the thermal efficiency of the energy tunnel involves two separate thermal loading modes. In winter, the energy tunnel acts as a heat source that can absorb heat from the ground to the surface of buildings. Conversely, it is a cooling source that transfers heat from the surface of buildings to the ground in summer. Therefore, the energy tunnel plays different roles in the heat transfer process throughout the year, resulting in a considerable impact on the overall heat transfer performance of the system. To minimize the head loss and ensure turbulent flow regime inside the pipes, and to optimize the difference between T_{out} and T_{s} (14 °C), T_{in} might be set as 4 °C in winter, and 28 °C in summer (Barla et al., 2016; Capozza et al., 2012). The loading time (60 d) in winter is calculated from November 15, 2011, while that in summer is calculated from June 1, 2011.

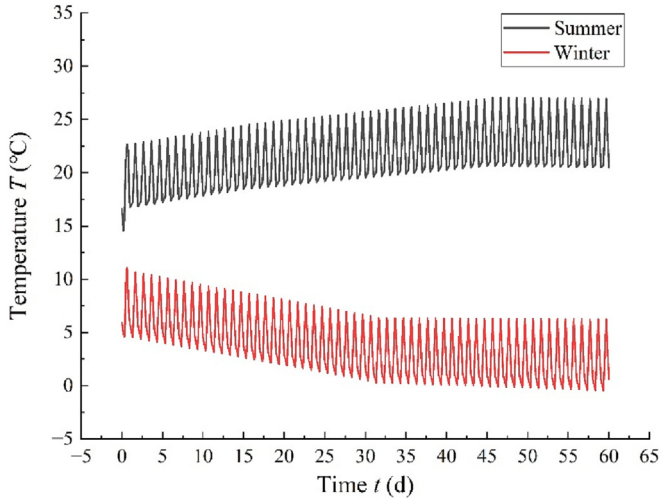

Fig. 5. Daily temperature in Turin, Italy (160 590 weather stations).

3 Results and discussion

3.1 Model calibration

The finite element model is first used to simulate the field test of the thermal efficiency of the Turin Metro Line Tunnel, as shown in Fig. 6. In winter when the outlet temperature is 4 °C higher than the injection temperature, geothermal energy acts as a heat source and can heat the energy segments. When the air velocity inside the tunnel is 0.1 m/s, the temperature at the outlet of the heat-carrying pipe is 7.28 °C, and the energy tunnel can provide 57.9 W heat per square meter on average. In summer, the outlet temperature is 23.7 °C below the injection temperature, and the energy tunnel acts as a cold source, which can absorb the heat from the heat-carrying fluid. The average cooling capacity per square meter of the tunnel lining is 74.7 W.

Figure 7 shows the temperature distribution of the ground and the tunnel in winter and summer, respectively. In general, after 60 days of thermal loading, there is no significant temperature change in the ground. However, under the influence of groundwater seepage flow, there is a certain degree of correlation between the temperature of the ground and the movement of groundwater. Along the seepage direction, the thermal influence area gradually expands, and the temperature gradually approaches the initial ground temperature. It can be seen that the temperature of the air inside the tunnel is about 6–10 °C lower or higher than the initial temperature of the ground. Due to the groundwater seepage flow, the change of the ground temperature is very limited, and geothermal mining in energy tunnels is, therefore, relatively efficient and stable.

The above simulation results are obtained based on the assumption that the ventilation velocity is equal to 0.1 m/s, but the actual ventilation conditions of the air inside the tunnel are variable. In general, the ventilation condition of 0.1 m/s is closer to the situation where there is no traffic in the tunnel. The effect of ventilation velocity on the thermal efficiency of the energy tunnel is also investigated. As shown in Fig. 8(a), for heating mode in winter, the ventilation velocity of the tunnel changes from 0.1 to 0.3 m/s (Barla et al., 2016), the outlet temperature of the heat-carrying pipes increases from 7.28 °C to 7.93 °C, and the heat exchange power increases by 11.47 W/m^2. In the cooling mode in summer, as shown in Fig. 8(b), if the air velocity is equal to zero, the outlet temperature of the heat-carrying pipes is as high as 25.6 °C, which is only 2 °C higher than the simulation result of 23.1 °C when the ventilation velocity is 0.2 m/s, and the heat transfer power is reduced by 35.0 W/m^2 for 60 days. Comparing the heat exchange power performance of the two different modes,

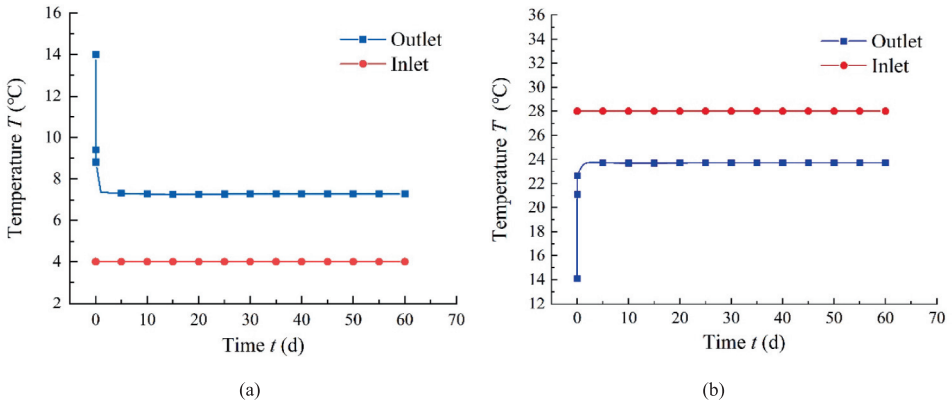

Fig. 6. Inlet and outlet temperature variation of heat-carrying pipes in (a) winter, and (b) summer.

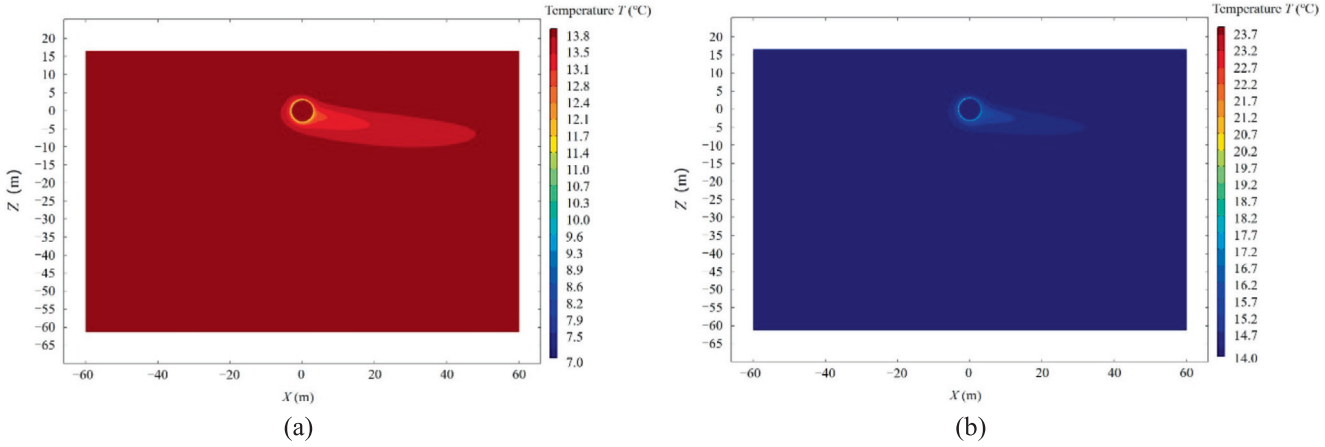

Fig. 7. Temperature distribution for (a) heating mode in winter, and (b) cooling mode in summer.

the increase in ventilation velocity can make the heat-carrying pipes obtain more heating/cooling capacity from the surrounding environment. The better the ventilation condition, the closer the air temperature inside the tunnel is to the ground temperature, and the more energy the heat-carrying pipes can absorb.

Barla et al. (2019) conducted a field test on the southern extension of the Turin metro tunnel in Italy. The research team proposed a complete energy segment testing and monitoring system. According to the on-site monitoring results, the average heat exchange power of the two rings of the energy tunnels is equal to 51.3 W/m^2. The error of the simulation results is about 12% higher than the experimental result, as shown in Table 4. This is probably due to the difference between the assumed ventilation velocity and the actual situation. With the gradual increase of the number of elements, the outlet temperature result is shown in Table 5.

3.2 Groundwater thermal convective analysis

According to the numerical results discussed above, it can be clearly recognized that the ground water flow has a great influence on the soil temperature field. In Fig. 9, assuming that the groundwater is in a static state and the groundwater level is still 12 m below the surface, the extracted heat for the heating mode is 50.1 W/m^2. In summer, the extracted heat power is 62.1 W/m^2. Compared with the previous simulation results, the total amount of geothermal energy extraction in one year is much smaller.

Figure 10 shows the effect of the groundwater flow velocity on the temperature distribution, where "Distance" represents the distance between the groundwater level and the central axis of the tunnel. For example, –6 m and 3 m mean that the groundwater level is 6 m below and 3 m above the central axis of the tunnel section, respectively. When the groundwater head position is below the tunnel, as shown in Fig. 10(a), the temperature distribution in the ground is still related to the direction of the groundwater flow. As the groundwater level increases, the groundwater flow begins to pass through the tunnel, as shown in Fig. 10(b)–(d), until the energy tunnel is completely embedded in the groundwater. It can be clearly observed that the ground with temperature changes is gradually expanding. The maximum horizontal influence area is about 20 m downstream of the groundwater flow in Fig. 10(a), while in Fig. 10(g), the influence area is extended to 40 m.

Figure 11 shows the relationship between the ground thermal conductivity and the extracted heat power. Under the heating mode, when the fluid inside the saturated soil is

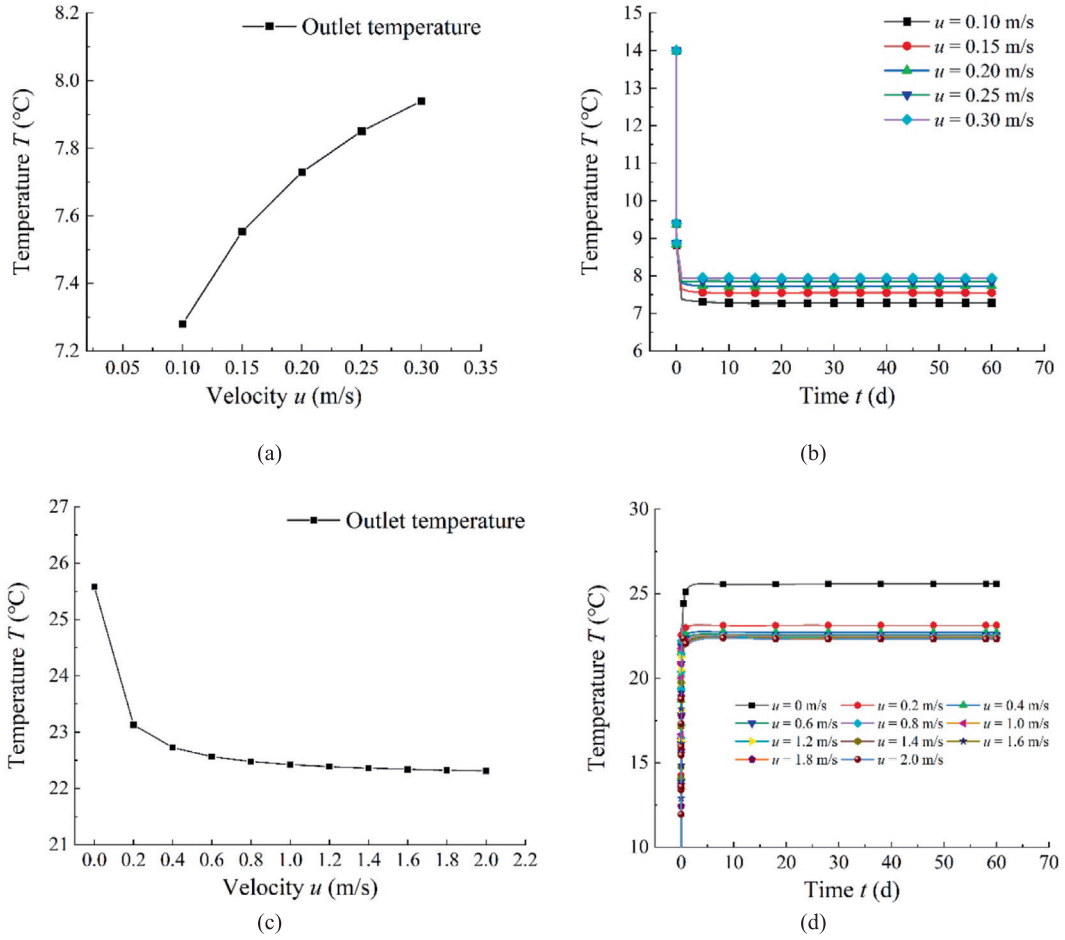

Fig. 8. Comparisons of seasonal outlet temperature under different ventilation conditions. (a), (b) The relationship between ventilation velocity and outlet temperature in winter, and (c), (d) the relationship between ventilation velocity and outlet temperature in summer.

Table 4
Comparison between numerical simulation and field test.

	Season	Q (W)	Q_A (W/m^2)	Q_L (W/m)
Numerical results	Winter	1.73	57.9	1 235.71
	Summer	2.23	74.7	1 595.28
Field test (Barla et al. 2019)	Winter	–	51.3	–

Table 5
Mesh sensitivity analysis.

	Outlet temperature at 60th day (°C)	Number of elements
1	7.2803	14 391
2	7.2537	15 037
3	7.1411	15 950
4	7.0505	17 020
5	7.0302	18 091
6	7.0162	19 236

in a static state, the geothermal energy produced by the system is relatively lower than the case considering groundwater flow. In addition, when groundwater seepage exists in the soil layer, the system has strong stability and is hard to be affected by the ground thermal conductivity. Therefore, it is easier for energy tunnels to run stably for a long time under the conditions of rich groundwater and developed seepage flow since the groundwater flow keeps the ground temperature stable, which can increase the thermal efficiency of the whole system.

Figure 12 shows the relationship between the heat exchange power and the initial ground temperature. The temperature of shallow geothermal water is usually not higher than 20 °C, and the sensitivity analysis is carried out by taking 8 °C—18 °C points with an interval of 1 °C. In winter, the higher the initial ground temperature is, the higher the thermal efficiency of the energy tunnel will be. In summer, a negative correlation between the heat exchange power and the initial ground temperature is observed. Hence, the initial ground temperature has differ-

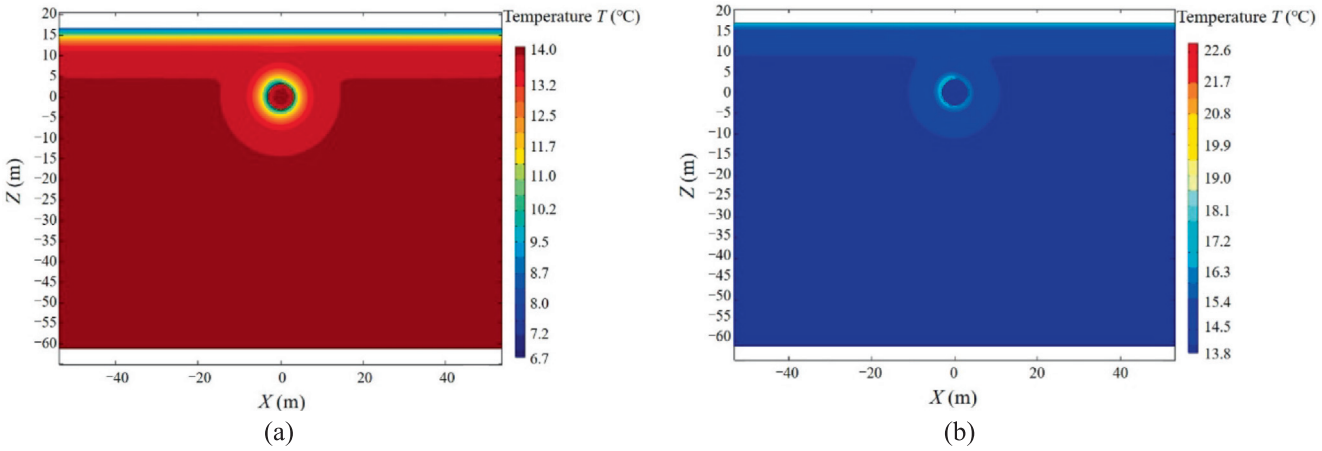

Fig. 9. Temperature distribution without groundwater flow. (a) Heating mode and (b) cooling mode.

ent effects on the thermal efficiency of the whole system in different seasons.

3.3 Parameter analysis and optimization

The effect of the heat-carrying pipes layout is investigated. Three different layouts are shown in Fig. 13. Layout 1, the one from the benchmark of Barla et al. (2016), is the normal condition that has been discussed above. Layout 2 and Layout 3 are characterized by that the main direction of the heat-carrying pipes is parallel to the circumferential direction of the tunnel. The length of the heat transfer pipes with a single ring lining segment is large, the distance between the pipes is small, and the heat-carrying fluid can sufficiently absorb heat or cold in the segment to reach the final convergence value. To compare the effects of the three different layouts, a series of parametric studies are performed.

The only heating in winter is operated because of the great demand for hot water among Chinese citizens. Moreover, the waste heat generated by the heavy and rapid traffic in the tunnel in summer temporarily increases the ambient temperature and inhibits the heat exchange of the heat exchanger, which opposes to energy tunnel system (heating in winter or cooling in summer). Figure 14 shows the extracted heat power in winter for the 3 different layouts. The inlet temperature of the heat-carrying pipes is 4 °C. The extracted heat power decreases sharply at the beginning due to the large temperature difference between the pipes and the surrounding environment (soil layer, tunnel, air, etc.), but soon they gradually tend to be stable. It is shown that the extracted heat power of Layout 2 upper circuit, about 68.3 W/m^2, is close to that of Layout 3, but the lower one of Layout 2 is very close to Layout 1, which has been confirmed by the similar temperature distribution of the heat-carrying pipes, as shown in Fig. 14(b)–(c). For Layout 1 (Barla et al., 2016), the extracted heat power of the numerical result is about 57.9 W/m^2, much lower than the other two layouts.

Figure 15 shows the schematic diagram of the pipeline parameters: $d_{\mathrm{inn,surf}}$, d_{lines} and theta, in which the red curve represents the heat-carrying pipe network. $d_{\mathrm{inn,surf}}$ represents the distance from the pipeline to the inner surface of the tunnel lining. d_{lines} represents the distance between the adjacent pipelines. Theta represents the position of the entrance and exit, clockwise.

Figures 16 and 17 show the thermal power results with the variation of $d_{\mathrm{inn,surf}}$, d_{lines} and theta, where the inlet temperature of the heat-carrying pipes is 4 °C. When $d_{\mathrm{inn,surf}}$ increases, which indicates that the heat-carrying pipes get closer to the air inside the tunnel, the heat output power per square meter of the tunnel lining increases gradually. When d_{lines} increases, an opposite change in the heat output power is observed. This is because larger distance between the pipes will induce the smaller number of the pipes installed on every square meter of the tunnel lining. The maximum heat output is about 88 W/m^2. Whereas, the effect of theta is very limited.

Figure 17 shows the thermal power optimization results with the variation of $d_{\mathrm{inn,surf}}$, d_{lines} and theta. Different from Fig. 16(a), the heat output power per meter of the pipe increases as d_{lines} increases. This is because a larger distance between the heat-carrying pipes will induce a higher thermal efficiency of each pipe. In addition, the effect of $d_{\mathrm{inn,surf}}$ and theta on the heat output power per meter of the pipe is like that in Fig. 16.

The Bobyqa optimization algorithm is used to optimize the thermal power based on the combined heating and cooling performance. The name Bobyqa is an acronym for Bound Optimization by Quadratic Approximation. The basic idea of the method is to iteratively approximate the objective function by a quadratic model which is valid in a region around the current iterate, the so-called trust region. The quadratic model is updated by minimizing the Frobenius norm of the difference in the Hessians of the two consecutive quadratic approximations. The angle of inlet/outlet pipes is among 0–360°. Considering the change in grid and the thickness of lining (300 mm), the

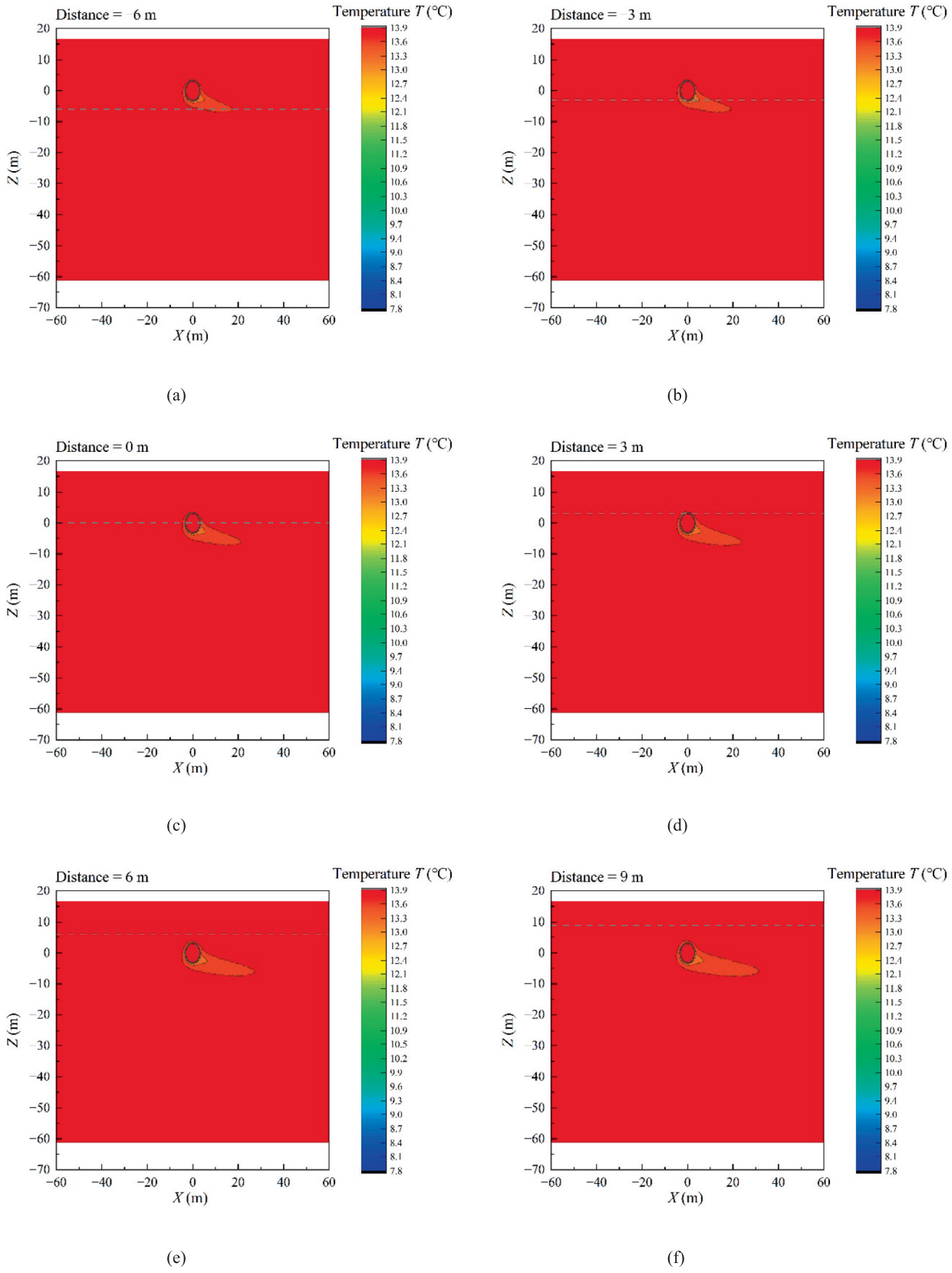

Fig. 10. Temperature distribution with different groundwater levels.

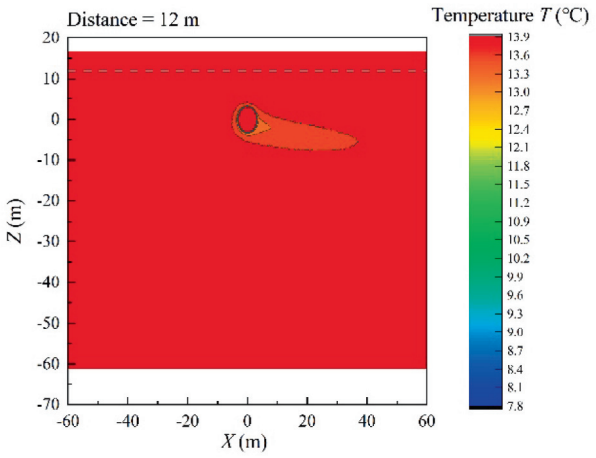

(g)

Fig 10. *(continued)*

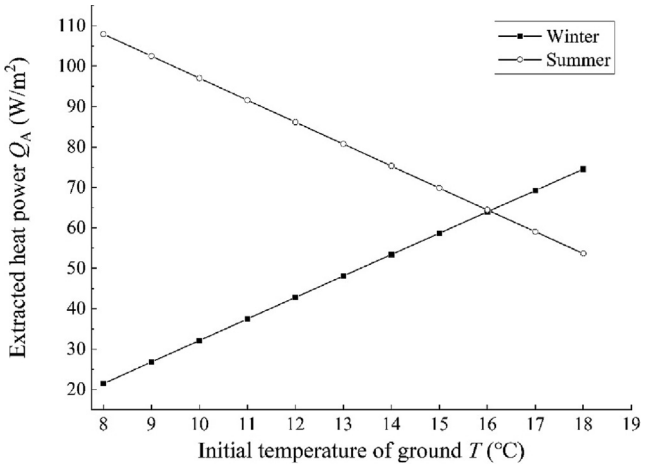

Fig. 12. Relationship between the heat exchange power and the initial ground temperature.

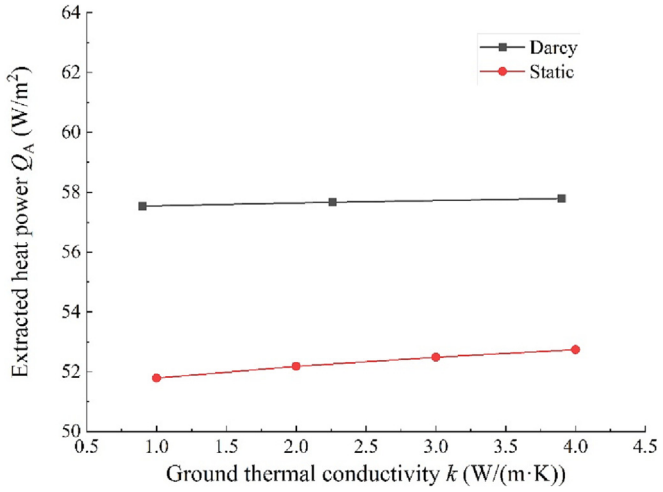

Fig. 11. Relationship between the ground thermal conductivity and the extracted heat power.

d_{lines} changes from 0.15 to 0.30 m, while $d_{inn,surf}$ varies from 0.10 m to 0.25 m.

The optimization goal is to obtain the highest thermal efficiency, which is embodied in solving the maximum heat transfer power per square meter of the tunnel linings. The optimization results are shown in Figs. 18–20. After optimization, the outlet temperature of 8.97 °C and the power of 87.2 W/m^2 can be obtained in the heating mode. In the cooling mode, the outlet temperature of 20.8 °C and the power of 126.34 W/m^2 can be obtained.

4 Discussion

The thermal efficiency of the energy tunnel heat exchanger depends on the relationship between the heat source and the geothermal energy. Since the temperature of the stratum is higher than that of the heat source in winter and lower than that of the heat source in summer, it can always meet the demand for water in social production and life and has high development potential. Although geothermal energy is used as a stable energy source to supply energy to the heat exchanger, thermal convection will occur in the air flow in the tunnel. When the air temperature is within the appropriate range (making the injected heat source meet the requirements of heating in winter and cooling in summer), the speed of thermal convection will also accelerate with the increase of air flow rate, as shown in Fig. 8. At this time, air convection plays a positive role in improving the heat transfer efficiency of the energy tunnel, otherwise, air convection will reduce the heat efficiency of the energy tunnel (such as the subway tunnel in summer).

Compared with the effect of air convection, the effect of groundwater is much more complex. Under the condition of continuous loading, the temperature field around the tunnel will be lower than the initial ambient temperature of the stratum, that is, it exists in the temperature disturbance area around the tunnel. Maximum performance improvements of respectively 149%, 127% and 49% can be achieved due to variations of the water table position, water flow velocity and water flow direction in this study (Ma et al., 2021b). With the increase of groundwater head height, the temperature disturbance area decreases, and the temperature field around the tunnel is closer to the initial temperature of the formation. However, the thermal influence area of groundwater will also increase, matched with the previous research (Ma et al., 2021b). The groundwater flow causes the dissipation of the temperature disturbance area, hence the geothermal mining in energy tunnels is relatively efficient and stable.

The optimization of the heat exchanger layout is a mathematical optimization of the existing basic geometry, but the result is still to retain the pre-set geometry. If the pipe-

(a) (b) (c)

Fig. 13. Three different layouts of the heat-carrying pipes. (a) Layout 1 (Barla et al., 2016), (b) Layout 2, and (c) Layout 3.

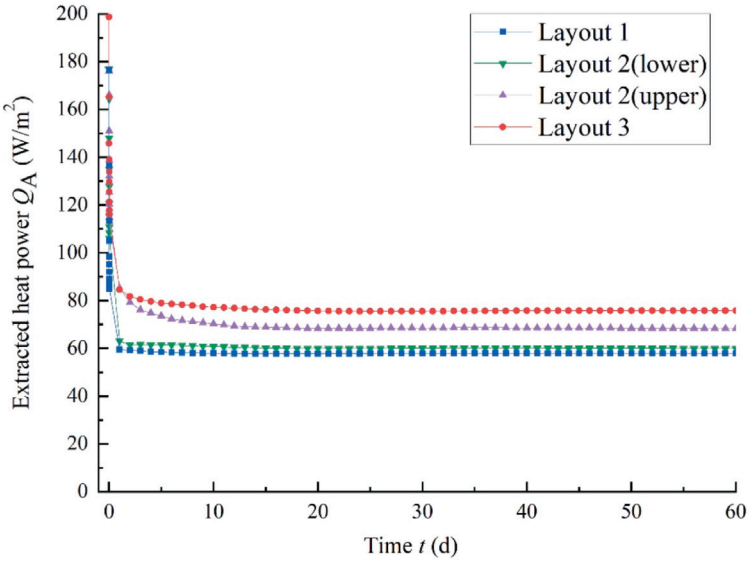

(a)

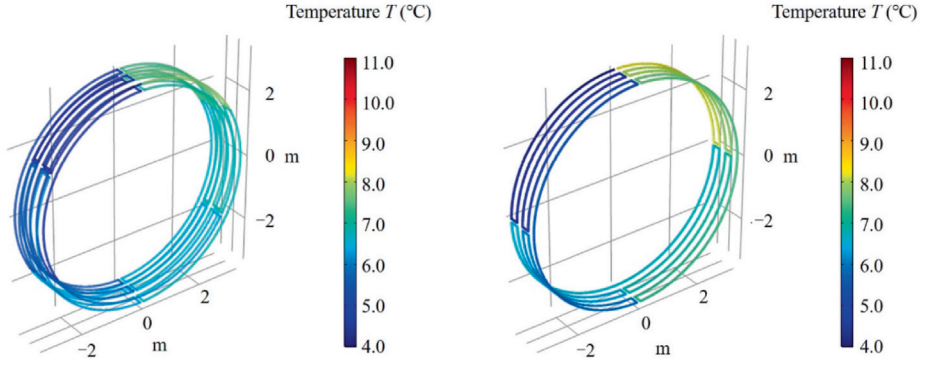

(b) (c)

Fig. 14. (a) Extracted heat power for three different modes, (b) temperature distribution of the heat-carrying pipes for Layout 2 (t = 60 d), and (c) temperature distribution of the heat-carrying pipes for Layout 3 (t = 60 d).

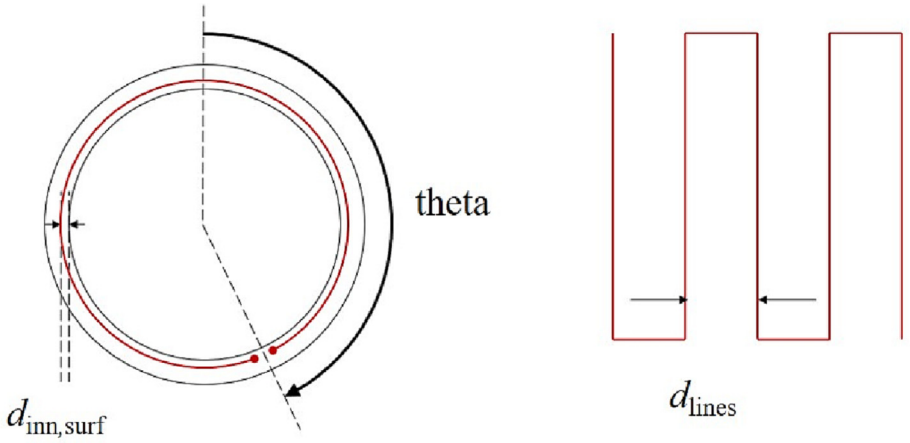

Fig. 15. Schematic diagram of pipeline parameters: $d_{inn,surf}$, d_{lines} and theta.

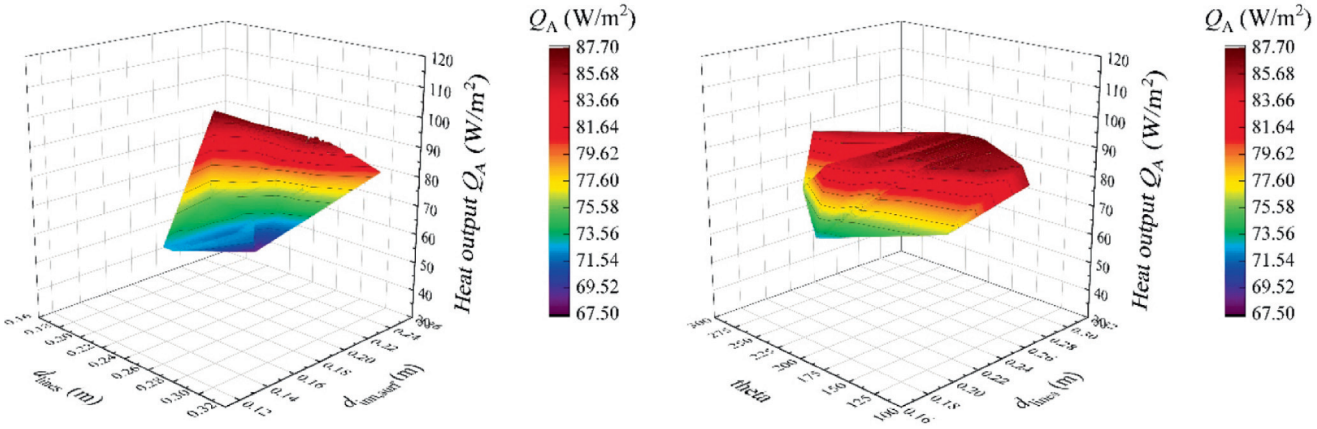

Fig. 16. (a) Effect of $d_{inn,surf}$ and d_{lines} on the heat output power per square meter of tunnel linings, and (b) effect of theta and $d_{inn,surf}$ on the heat output power per square meter of tunnel linings.

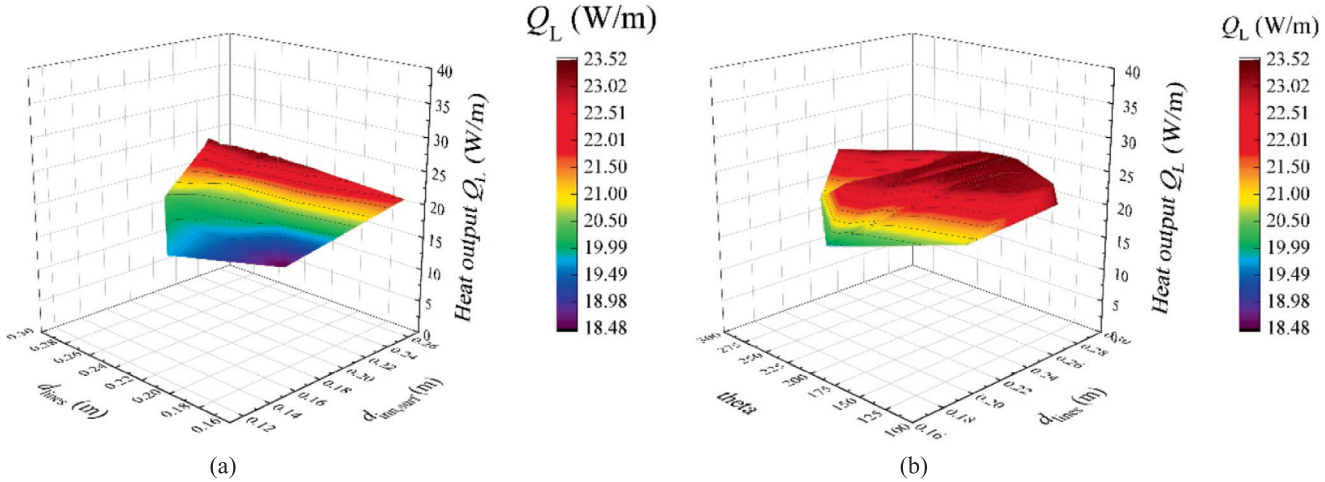

Fig. 17. (a) Effect of $d_{inn,surf}$ and d_{lines} on the heat output power per meter of the pipe, and (b) effect of theta and $d_{inn,surf}$ on the heat output power per meter of the pipe.

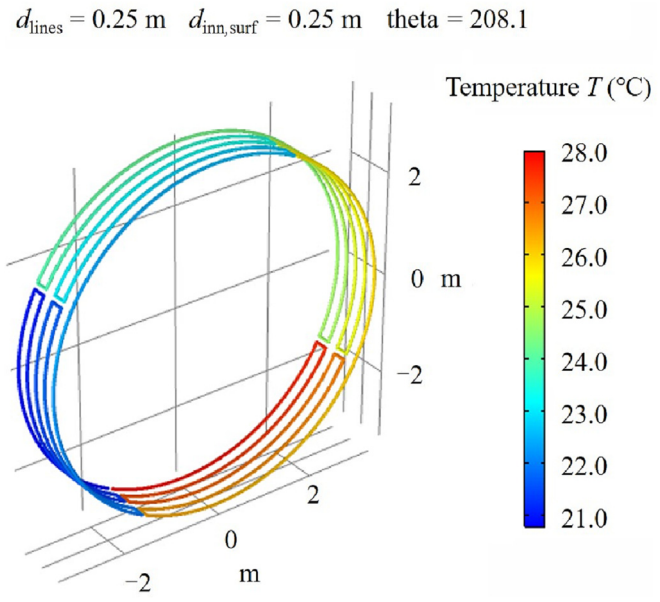

Fig. 18. Optimization results.

line layout can be optimized, several optimal basic layout forms can be determined, and then the results can be improved to adapt to the requirements of engineering construction and installation, and the overall efficiency can be improved. In addition, the air temperature only affects the inner surface of the linings. When the heat-carrying pipes are installed close to the inner surface, the thermal efficiency will increase sharply.

5 Conclusion

This study is the first attempt to research the optimization of pipe circuits in energy tunnels. A fully coupled thermo-hydraulic finite element model is built to investigate the response of tunnel-soil interaction under cyclical thermal loading. The main conclusions are as follows:

(1) The factors affecting the heat-carrying pipes include pipe location, pipe layout, soil thermal parameters, environmental conditions, etc., which are sensitive to the heat-transfer process of the heat source, the solum around it, and the ventilation of the tunnel. Air convection is very sensitive to the impact of the thermal efficiency of energy tunnels, and the groundwater environment plays a role in heat insulation.
(2) In the case of continuous injection of heat/cold sources, the temperature of the heat-carrying fluid in different parts of the tunnel lining gradually decreases/increases with the extension of the pipelines. Moreover, it will eventually become quasi-steady as time goes by.
(3) The relative relationship between the positions of heat-carrying pipelines will indeed affect the thermal efficiency of the entire energy tunnel system. The Bobyqa optimization algorithm is available for pipelines' geometric layout, and the optimization results show more heat efficiency than the initial ordinary layout.
(4) Considering the economic benefits and technical conditions, the impact of a single factor on thermal efficiency is limited. A reasonable solution, which comprehensively considers the factors affecting the boundary conditions, the thermal properties of the environment (soil layer, tunnel, air, etc.), and the layout of the heat-carrying pipes, will make a balance between the thermal efficiency and the installation cost.

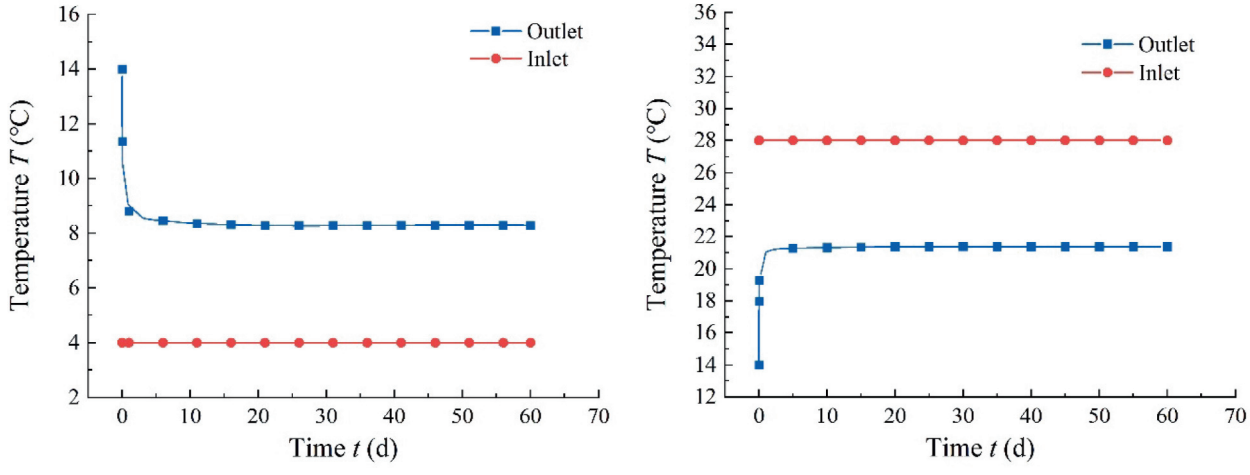

(a) (b)

Fig. 19. Inlet and outlet temperature variation of heat-carrying pipes in (a) winter, and (b) summer.

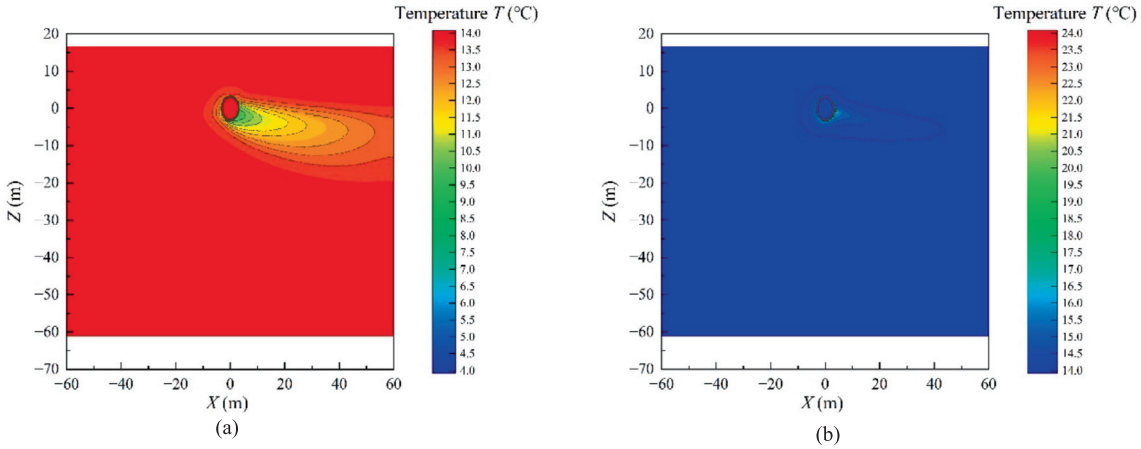

Fig. 20. Layout 3 temperature distribution for (a) heating mode in winter, and (b) cooling mode in summer. (t = 60 d).

Declaration of Competing Interest

The authors declare that they have no known competing financial interests or personal relationships that could have appeared to influence the work reported in this paper.

Acknowledgments

This research was supported by the Royal Society International Exchange, China (Grant No. IES\R1\211092), the China Postdoctoral Science Foundation (Grant No. 2019M651580). All the supports are acknowledged.

References

Agrawal, K. K., Agrawal, G. D., Misra, R., Bhardwaj, M., & Jamuwa, D. K. (2018). A review on effect of geometrical, flow, and soil properties on the performance of Earth air tunnel heat exchanger. *Energy and Buildings, 176*, 120–138.

Amis, T., Robinson, C. A. W., & Wong, S. (2010). Integrating geothermal loops into the diaphragm walls of the Bulgari Hotel Knightsbridge. In *Proceedings of the 11th DFI/EFFC International Conference London* (pp. 10).

Baralis, M., Barla, M., Bogusz, W., Di Donna, A., Ryżyński, G., & Żeruń, M. (2018). Geothermal potential of the NE extension Warsaw (Poland) metro tunnels. *Environmental Geotechnics, 7*(4), 282–294.

Barla, M., Baralis, M., Insana, A., Aiassa, S., Antolini, F., Vigna, F., Azzarone, F., & Marchetti, P. (2021). On the thermal activation of Turin metro line 2 tunnels. In *International conference of the international association for computer methods and advances in geomechanics* (pp. 1069–1076). Cham: Springer.

Barla, M., & Di Donna, A. (2018). Energy tunnels: Concept and design aspects. *Underground Space, 3*(4), 268–276.

Barla, M., Di Donna, A., & Insana, A. (2019). A novel real-scale experimental prototype of energy tunnel. *Tunnelling and Underground Space Technology, 87*, 1–14.

Barla, M., Di Donna, A., & Perino, A. (2016). Application of energy tunnels to an urban environment. *Geothermics, 61*, 104–113.

Brandl, H. (2006). Energy foundations and other thermo-active ground structures. *Géotechnique, 56*(2), 81–122.

Buhmann, P., Moormann, C., Westrich, B., Pralle, N., & Friedemann, W. (2016). Tunnel geothermics—A German experience with renewable energy concepts in tunnel projects. *Geomechanics for Energy and the Environment, 8*, 1–7.

Capozza, A., De Carli, M., Galgaro, A., & Zarrelle, A. (2012). *Guidelines for the design of geothermal fields for heat pumps*. Italy: Padova (in Italian).

Di Donna, A., & Barla, M. (2016). The role of ground conditions on energy tunnels' heat exchange. *Environmental Geotechnics, 3*(4), 214–224.

Franzius, J. N., & Pralle, N. (2011). Turning segmental tunnels into sources of renewable energy. *Proceedings of the institution of civil engineers-civil engineering* (Vol. 164(1), pp. 35–40). Thomas Telford Ltd.

Insana, A., & Barla, M. (2020). Experimental and numerical investigations on the energy performance of a thermo-active tunnel. *Renewable Energy, 152*, 781–792.

Lee, C., Park, S., Won, J., Jeoung, J., Sohn, B., & Choi, H. (2012). Evaluation of thermal performance of energy textile installed in Tunnel. *Renewable Energy, 42*, 11–22.

Li, C., Zhang, G., Zhang, Q., Xie, Y., Liu, X., Cao, S., & Wei, B. (2022). Preliminary design method for absorber pipe length of tunnel lining ground heat exchangers based on energy efficiency of heat pump. *Underground Space, 7*(6), 1156–1174.

Liu, X., Li, C., Zhang, G., Zhang, L., & Wei, B. (2021). Numerical investigation on energy efficiency of heat pump with tunnel lining ground heat exchangers under building cooling. *Buildings, 11*(12), 611.

Ma, C., Di Donna, A., Dias, D., & Zhang, J. (2021). Numerical investigations of the tunnel environment effect on the performance of energy tunnels. *Renewable Energy, 172*, 1279–1292.

Ma, C., Di Donna, A., Dias, D., & Zhang, T. (2021). Thermo-hydraulic and sensitivity analyses on the thermal performance of energy tunnels. *Energy and Buildings, 249*,, 111206.

Makasis, N., & Narsilio, G. A. (2021). A case study on the application of energy tunnels in Sydney, Australia. In *International conference of the international association for computer methods and advances in geomechanics* (pp. 1077–1084). Cham: Springer.

Nicholson, D. P., Chen, Q., de Silva, M., Winter, A., & Winterling, R. (2014). The design of thermal tunnel energy segments for Crossrail, UK. In *Proceedings of the Institution of Civil Engineers-Engineering Sustainability* (pp. 118–134). Thomas Telford Ltd.

Ogunleye, O., Singh, R. M., & Cecinato, F. (2021). Assessing the thermal efficiency of energy tunnels using numerical methods and Taguchi statistical approach. *Applied Thermal Engineering, 185*, 116377.

Rowland, J. (2019). *Making use of metro heat [M/OL]*. Tunneltalk, https://www.tunneltalk.com/TunnelTECH-08Aug2019-Metro-heat-recovery-research.php.

Shafagh, I., Rees, S., & Loveridge, F. (2020). Investigations into thermal resistance of tunnel lining heat exchangers. *E3S Web of Conferences, Vol. 205*.

Song, H., Pei, H., & Zhang, P. (2023). Probabilistic method for the size design of energy piles considering the uncertainty in soil parameters. *Underground Space, 10*, 37–54.

Tinti, F., Boldini, D., Ferrari, M., Lanconelli, M., Kasmaee, S., Bruno, R., Egger, H., Voza, A., & Zurlo, R. (2017). Exploitation of geothermal energy using tunnel lining technology in a mountain environment. A feasibility study for the Brenner Base tunnel – BBT. *Tunnelling and Underground Space Technology, 70*, 182–203.

Tsagarakis, K. P., Efthymiou, L., Michopoulos, A., Mavragani, A., Anđelković, A. S., Antolini, F., Bacic, M., Bajare, D., Baralis, M., Bogusz, W., & Burlon, S. (2020). A review of the legal framework in shallow geothermal energy in selected European countries: Need for guidelines. *Renewable Energy, 147*, 2556–2571.

Zannin, J., Ferrari, A., Pousse, M., & Laloui, L. (2021). Hydrothermal interactions in energy walls. *Underground Space, 6*(2), 173–184.

Zhang, G., Cao, Z., Zhao, X., Xie, Y., Liu, X., & Cao, S. (2021). Investigation of the thermal performance of energy tunnel equipped with the insulation layer considering ventilation and groundwater seepage. *Geofluids, 2021*, 6021585.

Zhang, G., Guo, Y., Zhou, Y., Ye, M., Chen, R., Zhang, H., ... Liu, C. (2016). Experimental study on the thermal performance of tunnel lining GHE under groundwater flow. *Applied Thermal Engineering, 106*, 784–795.

Zhu, Z., & Guo, H. (2019). Exploration on construction of geothermal–utilized shield tunnels: A case study of fabrication and installation of tunnel energy segments in Qinghuayuan Tunnel. *Tunnel Construction, 39*(4), 677–683.